THE ASTROPHYSICAL JOURNAL, 379:639–646, 1991 October 1

STAR COUNTS AND CARBON MONOXIDE OBSERVATIONS OF MADDALENA'S CLOUD

YOUNGUNG LEE, RONALD L. SNELL, AND ROBERT L. DICKMAN
Five College Radio Astronomy Observatory, Department of Physics and Astronomy, University of Massachusetts, Amherst, MA 01003
Received 1991 January 7; accepted 1991 April 11

ABSTRACT

We have mapped the inner region of Maddalena's cloud, a massive, cold object in the outer Galaxy, in both ^{12}CO and ^{13}CO ($J = 1$–0) using the FCRAO 14 m telescope. The visual extinction has been determined by star counts and is used to investigate the gas and dust properties of the cloud.

Our results indicate that the ^{13}CO column density to visual extinction ratio is similar to that found in local molecular clouds. This suggests that if the gas to dust ratio is normal, the CO abundance is similar to that of the clouds near the Sun. The masses derived from the LTE and virial analyses differ by a factor of 5; the virial analysis gives a mass 5 times larger than the LTE value. The structure and kinematics of the cloud inferred from the CO maps suggest that the inner region of the cloud may be expanding. Thus, both the kinematics of the cloud and the mass discrepancy suggest that this object may not be gravitationally bound. If we assume the LTE mass to be correct, the ratio of molecular hydrogen column density to CO integrated intensity is 0.7×10^{20} cm^{-2} (K km s^{-1})$^{-1}$, much lower than that found for most GMCs in the inner Galaxy.

Subject headings: interstellar: molecules

1. INTRODUCTION

Giant molecular clouds (GMCs) in our Galaxy are a significant mass component of the interstellar medium. However, investigations of these objects often suffer from an observational bias: usually the clouds selected for study are located near H II regions, OB associations, bright IR sources, or other recent products of the formation of fairly massive stars. Little attention has been given to clouds that show no conspicuous star-forming activity, although there is evidence that such clouds exist. Comparing the unbiased Columbia CO survey of distant objects in the inner Galaxy with far-infrared, radio-continuum, and radio recombination line surveys, Myers et al. (1986) showed that the number of young stars that accompany large molecular clouds fluctuates greatly and that some large clouds display little or no evidence of star formation. Using the Massachusetts-Stony Brook Galactic Plane CO Survey, Solomon, Sanders, & Rivolo (1985) identified 2000 CO emission centers. These separated into two populations according to temperature, which they labeled as cold clouds and warm clouds. They found that the cold clouds must be more widespread both in and out of spiral arms, than the warm clouds. More importantly, they found that three-quarters of the emission centers were cold. Thus, cold, giant molecular clouds may be quite numerous in the Galaxy.

A large molecular cloud in the third quadrant at Galactic coordinates $l = 216.^\circ5$, $b = -2.^\circ5$, was identified in the Columbia CO survey by Maddalena & Thaddeus (1985; hereafter we call it Maddalena's cloud). The cloud was estimated to have a mass of $\sim 10^6\ M_\odot$ and was distinguished by being very cold, with no optical or infrared signs of star formation, They suggested that the cloud may be relatively young and has not yet extensively formed stars, based on their ^{12}CO and radio continuum data. However, the resolution of the Columbia CO survey (8.′7 beamwidth) was not adequate to determine the structure of the cloud, and no higher resolution observations in any molecular species have been published, leaving unresolved the extent with which this cloud or any of the cold, giant molecular clouds differ from other GMCs.

There are several advantages in studying Maddalena's cloud as opposed to cold clouds in the inner Galaxy; first, a distance can be estimated from its radial velocities, unlike the situation in the inner Galaxy, second, Maddalena's cloud is much closer than other known massive clouds in the inner Galaxy; and last, source confusion, which complicates the analysis of clouds, is less significant in the outer Galaxy.

In this paper we present the first high angular resolution maps of ^{12}CO and ^{13}CO emission from the inner region of Maddalena's cloud. We have also made the first determination of the visual extinction distribution in this cloud using star counts. This provides the first estimate of the ^{13}CO column density to extinction ratio in a molecular cloud outside the solar neighborhood. This study is the first step of a project to fully map Maddalena's cloud (18 deg^2) with 50″ sampling. Observations of the CO and the star count method are described in § 2. In § 3 we present the results of the observations. In § 4 we discuss the correlation between visual extinction and ^{13}CO column density, and the physical parameters derived for the cloud including velocity field. In § 5 we summarize our results.

2. OBSERVATIONS OF CO AND THE STAR COUNTS METHOD

2.1. CO *Observation*

A 1 deg^2 region of Maddalena's cloud ($l = 216.^\circ0$ to $217.^\circ0$, $b = -2.^\circ0$ to $-3.^\circ0$) was mapped in the $J = 1$–0 transition of ^{12}CO and ^{13}CO between 1989 December and 1990 February, using the 14 m telescope of the Five College Radio Astronomy Observatory. The sampling was 3′ and the FWHM beam size was 45″ at 115.27 GHz and 47″ at 110.2 GHz. A 0.25 deg^2 region centered on the strongest emission in the 1 deg^2 region ($l = 216.^\circ45$ to $216.^\circ95$, $b = -2.^\circ45$ to $-2.^\circ95$) was remapped with a spacing of 1′ in the same transitions of both ^{12}CO and ^{13}CO. All observations were made by position switching between the observed positions and a reference position located at $l = 216.^\circ5$, $b = -4^\circ$. Each reference observation was shared with observations of four positions within the map. Calibration was accomplished by frequently observing an ambient temperature load. All antenna temperatures quoted are corrected for atmospheric extinction and for the forward

spillover and scattering losses of the antenna and radome, and are therefore on the T_R^* temperature scale defined by Kutner & Ulich (1981). Two 256 channel filter banks with spectral resolutions of 250 and 100 kHz were used, which provided resolutions of 0.65 and 0.26 km s^{-1}, respectively, at the frequency of ^{12}CO. The data were smoothed and resampled at 1 km s^{-1} resolution. The 0.25 deg^2 region mapped with 1′ sampling had a 1 σ rms noise in ^{12}CO and ^{13}CO of 0.28 and 0.18 K; the 1 deg^2 region with 3′ sampling had rms noise of 0.33 and 0.19 K, respectively.

2.2. *Star Counts*

The basic procedure used for the star counts follows that given by Bok & Cordwell (1973) and Dickman (1975, 1978b). Star counts were made by superposing a transparent grid ("reseau") with rulings every 2.′2 × 2.′2 (2 × 2 mm) on the Palomar Observatory Sky Survey red print. Stars were counted in each grid element of a 0.25 deg^2 region, using a 30 × microscope. Red and blue prints of three reference fields were counted at adjacent positions, in order to determine the unextincted star density. All stars in a given reseau square were counted, with no attempt to sort them into magnitude intervals based upon image size. We repeated the counts twice to check for counting constancy. Positioning and alignment errors were minimized by several procedures utilizing computer-generated transparent plate overlays, and it is estimated that as a result of these precautions the error in the location of any reseau square is less than 0.′2. The extinctions for each square derived from the star counts are computed relative to the nearby reference fields. The presence of any residual obscuration in the reference fields leads to a systematic underestimate of the background stars and thus, of cloud extinction.

3. RESULTS

3.1. *Distance*

An accurate distance determination is important for estimating the number of foreground stars used for deriving the cloud extinctions, and for estimating cloud parameters, such as size, mass, and luminosity. Kinematic distances of 2.7 and 2.14 kpc have been estimated by Maddalena & Thaddeus (1985) and Sodroski (1991); the differences arise due to the use of slightly different rotation curves and cloud radial velocities. However, due to uncertainties in the rotation curve in the outer Galaxy, the fact that the cloud lies near the anticenter, and the random motions of clouds, the distance to Maddalena's cloud is not well established by kinematics.

Using a model of the Galactic radial velocity field (Feitzinger & Spicker 1987), Neckel et al. (1989) obtained a distance of 2.3 kpc for S287 (or NS14) close to Maddalena's cloud; the H II region has a radial velocity nearly identical to Maddalena's cloud. They also estimated a photometric distance of 2.1 kpc for S287. The agreement between the radial velocities of Maddalena's cloud and the molecular cloud associated with the H II region suggests the two are at the same distance.

Another method for estimating distance is based on the reddening of bright stars (see, for example, Snell 1981). Given MK spectral types, visual magnitudes, and $(B-V)$ colors for the stars in the vicinity of a cloud, one can calculate their color excess, E_{B-V}, and distance, based upon the intrinsic color $(B-V)_0$ and absolute magnitude associated with their spectral type and luminosity class. Figure 1 shows a plot of color excess versus distance for 42 stars in the vicinity of Maddalena's cloud; since MK spectral data and colors are available for only a rather limited number of stars from the Kennedy & Buscombe Catalog (1977), quite a large area (7.°5 × 6°) had to be employed to obtain this sample. Figure 1 shows that at a distance of approximately 2 kpc there is a rapid rise in the visual extinction.

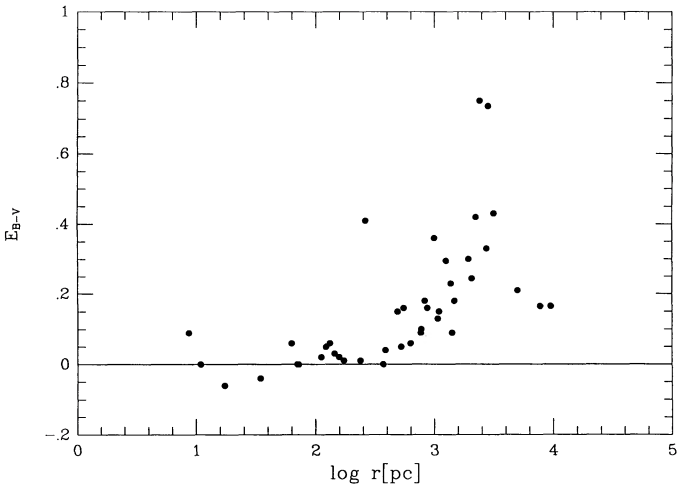

FIG. 1.—Color excess vs. distance for 42 stars in the vicinity of Maddalena's cloud.

In consideration of uncertainties the distances are all in reasonable agreement. By combining all the above estimates, we thus adopt 2.2 kpc as the distance of Maddalena's cloud.

3.2. CO *Column Density*

The column density of ^{13}CO at each map position may be estimated from our observations of the ^{12}CO and ^{13}CO line temperatures and from the line width of the ^{13}CO emission, assuming LTE (Dickman 1978a; Penzias 1975). These measurements allow us to determine the excitation temperature and the ^{13}CO optical depth. With the LTE assumptions, the column density of ^{13}CO in the ith pixel of a cloud is given

$$N(^{13}CO)_i = \frac{2.42 \times 10^{14} \Delta V_i T_x \tau^{13}}{1 - \exp\left[-5.29/T_x\right]} \left[\mathrm{cm}^{-2}\right], \qquad (1)$$

where τ^{13} is the line optical depth of ^{13}CO, T_x is the excitation temperature, and ΔV_i is the full width at half-intensity in velocity units. Above equation was used for the pixels with emission in ^{13}CO larger than the 3 σ noise level. For pixels with emission weaker than the 3 σ noise level, we assumed optically thin emission and used the integrated intensity of ^{13}CO:

$$N(^{13}CO)_i = \frac{3.76 \times 10^{14}}{f_u} \int T_R^*(^{13}CO) dv \left[\mathrm{cm}^{-2}\right], \qquad (2)$$

where f_u is the fraction of ^{13}CO in the upper state ($J = 1$). We take $f_1 = 0.55$, assuming $T_x = 5$ K. Most of column density, and thus mass, are produced in regions with strong ^{13}CO emission. Assuming a $[H_2]/[^{13}CO]$ abundance ratio of 5×10^5 (Dickman 1978a; see also § 4.1), we can then determine the H_2 column density and total mass (LTE masses derived in this manner are multiplied by a factor of 1.36 to account for the contribution of He by mass). A contour map of $N(^{13}CO)$ is shown in Figure 2*a* for the 0.°5 × 0.°5 region that was sampled every 1′. The map has been smoothed to the resolution of star counts, 2.′2. Column densities shown range from 1 to 8 × 10^{15}

cm^{-2}. The peak ^{13}CO column density of 8×10^{15} cm^{-2} is a lower limit, as it is smoothed over larger area than the telescope beam; the peak ^{13}CO column density before smoothing was 12.4×10^{15} cm^{-2}.

3.3. *Visual Extinction*

Determining extinctions in distant clouds using star counts is made difficult by the presence of foreground stars. A completely opaque region, which in a nearby cloud will show a total absence of stars, becomes increasingly difficult to distinguish at progressively larger distances, since the presence of interposed foreground stars reduces the contrast between the cloud and the unobscured, adjacent sky. Accordingly, once star counts have been carried out on a distant object, the raw counts in each reseau element must be reduced by the mean number of foreground stars expected within the solid angle subtended by each grid element at the distance of the cloud. Note that this procedure invariably reduce the dynamic range of the counts and, owing to the reduction in star numbers, unavoidably increases the statistical ($\sqrt{n}$) errors associated with the counts. We have generally followed the Herbst & Sawyer (1981) method for estimating foreground stars. They calculated foreground star numbers for samples of distant opaque clouds within $b = \pm 10°$ as well as those of nearby clouds, using the following method. The fundamental equation of general star-count analysis for an opaque cloud at distance r may be written as

$$N_{ct} = \omega \int_{-\infty}^{m_{lim}} \int_{0}^{r} D(r') \times \Phi[m - 5 \log r' + 5 - E(r')] r'^2 \, dr' \, dm \,, \quad (3)$$

where N_{ct} is the number of stars counted, ω is the solid angle and m_{lim} is the limiting magnitude of the counts. The quantity $D(r)$ represents the volume density of stars at distance r in units of the corresponding stellar density near the Sun, $\Phi(M)$ is the luminosity function, and $E(r)$ is the extinction out to r along the line of sight. In the present case, the limiting magnitude is estimated to be 20.5 mag, based on an extrapolation of the van Rhijn (1929) tables. By using observed values of N_{ct}, such as those of van Rhijn (1929), equation (3) can be solved analytically for $D(r)$ by differentiating both sides with respect to r. Unfortunately, such a method is impractical. However, an average density of stars can be determined from star counts to a known limiting magnitude in the direction of an opaque cloud. For NGC 2175 at a distance and direction ($d = 2.1$ kpc; $l = 190°$, $b = 0°$) similar to those of Maddalena's cloud, Herbst & Sawyer (1981) calculated averaged density of stars $\langle D(r) \rangle = 0.25$, wherein the reddening is assumed to be evenly distributed along the line of sight.

Using equation (3) with the adopted general extinction of $E_{B-V} = 0.1$ from Figure 1, an average density of 0.25, a cloud distance of 2.2 kpc, and the luminosity function of Wielen, Jahreiss, & Krüger (1983), we estimate the number of foreground stars in 2'.2 × 2'.2 reseau as 6.8. We are able to compare our value to that of NGC 2175 ($d = 2.1$ kpc, $l = 190°$, $b = 0°$), 5.7, and that of IC 1085 ($d = 2.4$ kpc, $l = 136°$, $b = +2°$), 7.1 (Herbst & Sawyer 1981). In consideration of their limiting magnitude of 21.1, our value of 6.8 seems to be a proper one.

The visual extinction distribution is shown as a gray (and contour) scale map in Figure 2*b*. An inspection of Figures 2*a* and 2*b* shows a good correlation between ^{13}CO emission and visual extinction. Condensations with $A_V \geq 3$ magnitudes are visible, and a hole appears around the central portion of the cloud ($l = 216°.7$, $b = -2°.65$) in both maps. Some differences appear in the lower right and central parts of the map, possibly caused by noise in the data. Comparing visual extinction map with the integrated intensity map of ^{13}CO emission (Fig. 2*c*) and ^{12}CO peak temperature map (Fig. 2*d*), the apparent thickness and shape of the cloud are found to be in generally good agreement in all three maps. Note that the maps of visual extinction and ^{13}CO column density have 2'.2 resolution, and the maps of ^{12}CO peak temperature and ^{13}CO integrated intensity have 1' resolution.

3.4. *Kinematics and Masses*

Figure 3 shows the cloud's velocity field over the entire 1° × 1° region mapped. The cloud has an interesting velocity structure that is best seen in maps of the ^{12}CO emission in Figure 3. A systematic velocity shift is seen across the cloud; the lowest velocity emission is found primarily in the southeast, while the highest velocity emission is found in the northwest. At intermediate velocities (24 ~ 26 km s^{-1}) a nearly complete ring is seen. The explanation for this velocity gradient may be either rotation or expansion of the cloud about a center located at $l = 216°.5$, $b = -2°.5$. As we show later, interpretation of the velocity gradient as an expansion appears to be consistent with several other unusual properties of the cloud. The spectra presented in Figure 4 suggest that there is additional structure in the velocity field; some parts of the 1 deg^2 core region show clear double- or triple-peak spectra. This cloud is unlikely to be blended, according to the *l*–*v* map of Maddalena & Thaddeus (1985), so that these features reflect the velocity field of a single object.

If we assume a uniform density distribution, the virial mass of Maddalena's cloud is given by $M_{vir} = 5\sigma_{tot}^2 D/2G$, where D is the diameter and σ_{tot} is the one dimensional velocity dispersion. In estimating the velocity dispersion, two types of gas motions within the molecular cloud must be considered (Dickman & Kleiner 1985; Lee, Snell, & Dickman 1990): σ_i, an "internal dispersion" which represents the spread of velocity observed along each line of sight, and σ_c, a "centroid dispersion" which represents bulk motion of gas within the cloud. Thus, the total magnitude of velocity fluctuations is given by $\sigma_{tot}^2 = \sigma_i^2 + \sigma_c^2$. To avoid the possibility of saturation effects on the ^{12}CO line widths, we used ^{13}CO in calculating the velocity dispersion.

Two methods were used to determine cloud masses. The virial mass of the 0.25 deg^2 region mapped in this study is estimated to be 7.7×10^4 $M_\odot$, and the LTE mass is estimated to be 1.0×10^4 $M_\odot$. The virial mass is a factor of 8 larger than the LTE mass. For the 1 deg^2 region of the cloud, the virial mass is 1.2×10^5 $M_\odot$, and the LTE mass is 0.25×10^5 $M_\odot$; the virial mass is a factor of 5 larger than the LTE mass, and the discrepancy is similar to that for the smaller region.

4. DISCUSSION

4.1. *Visual Extinction versus* ^{13}CO *Column Density*

Figure 5 shows the observed correlation of $N(^{13}CO)$ versus A_V. A regression line to describe the relationship between these quantities can be obtained in many ways (Isobe et al. 1990), including the usual least-squares fit, which minimizes the quantity $\Sigma[N(^{13}CO)_i - aA_V - b]^2$, where $N(^{13}CO)_i$ and A_V are individual values of column density and visual extinction, and a and b are the slope and the intercept of the fitted line. This

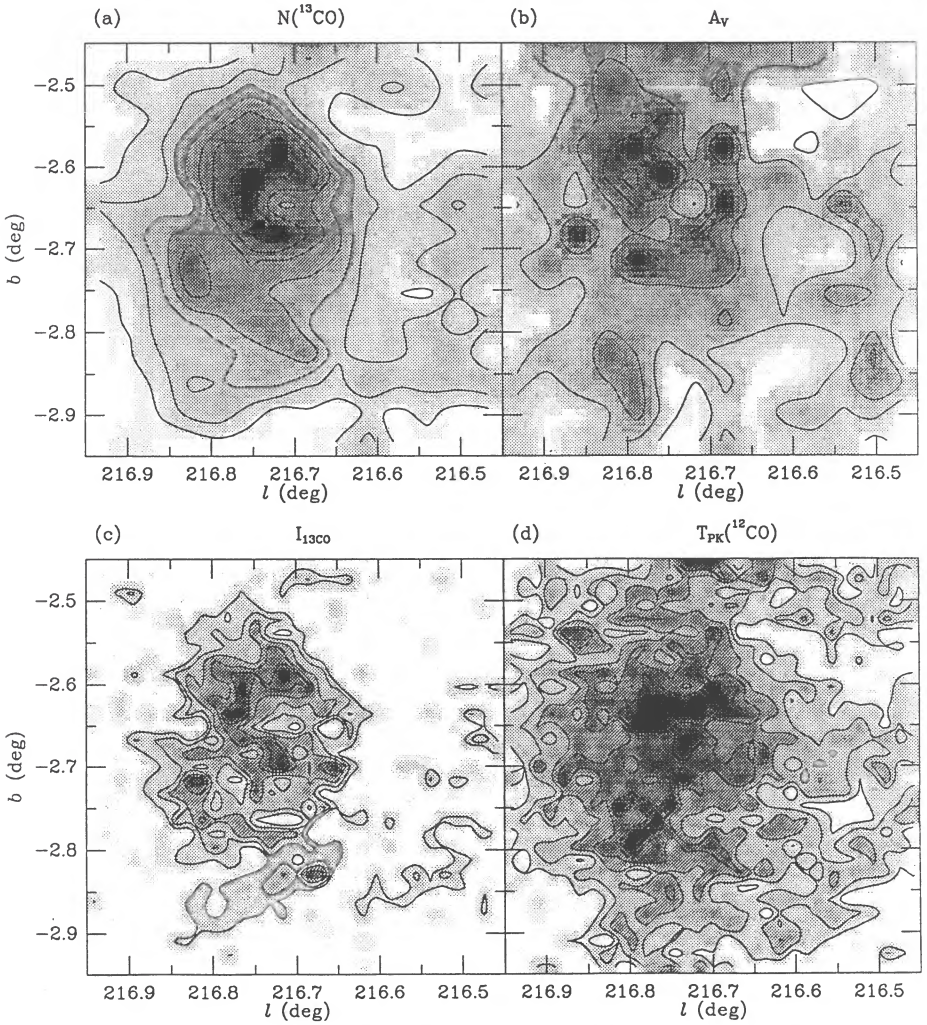

FIG. 2.—(*a*) ^{13}CO column density map of the 0.25 deg^2 region of Maddalena's cloud with 2.′2 resolution; contour levels are 1, 2, 3, ..., 8 × 10^{15} cm^{-2}. (*b*) Visual extinction map with 2.′2 resolution; Contour levels are 1, 2, 3, 4, and 5 mag. (*c*) ^{13}CO integrated intensity map with 1′ resolution; contour levels are 3, 4, 5, ..., 9, 10 K km s^{-1}. (*d*) ^{12}CO peak temperature map with 1′ resolution; contour levels are 2, 2.5, 3, ..., 4.5, 5 K.

method, however, fixes the x-axis, A_V, and sometimes gives an unrealistic fit. The results of this fit to the data is shown by the dotted line in Figure 5. The points have large dispersion, but this is expected, since we have applied star counts to an object a factor of 4 or 5 more distant than clouds in the solar neighborhood.

One can exchange the axes $N(^{13}\mathrm{CO})_i$ and A_V with each other, and minimize the quantity $\Sigma[A_V - aN(^{13}\mathrm{CO})_i - b]^2$. In this case, the ^{13}CO column density is fixed. The regression line of A_V on $N(^{13}\mathrm{CO})$ is shown as the dashed line in Figure 5 and is given by $N(^{13}\mathrm{CO}) = 3.0 \times 10^{15}(A_V - 1.5)$.

If the two parameters in a regression fit have a good correlation, the slopes obtained by the above two ways are, ideally, inversely proportional to each other. However, in most cases, the two slopes are not inversely matched precisely, because the two-fit parameters will typically have different error ranges. Recently, Isobe et al. (1990) showed that these two slopes are the two extreme cases in a more general fit; one has the steepest slope and the other the smallest. Isobe et al. (1990) also introduced three other fits and calculated the dispersion of those slopes. They suggest that the bisector of the two extreme slopes performs significantly better than the other methods. In adopting their technique, we have therefore used traditional least-squares fits to obtain the bisector regression line, which is given by

$$N(^{13}\mathrm{CO}) = (1.73 \pm 0.09) \times 10^{15}(A_V - 0.95)\,. \qquad (4)$$

The bisector fit is shown as the solid line in Figure 5.

In Table 1 the slopes and intercepts of various published regression lines of column densities relative to visual extinctions for nearby clouds are listed. Slopes range from 1.3 × 10^{15} to 3.8 × 10^{15} cm^{-2} mag^{-1} and Dickman & Clemens (1983) derived 1.9 × 10^{15} cm^{-2} mag^{-1} for a large sample of local dark clouds. Since the slopes given in Table 1 were obtained by least-squares fits, they should be regarded as lower limits, according to Isobe et al. (1990). In any case our results indicate that the ^{13}CO column density to visual extinction ratio in Maddalena's cloud is similar to (or slightly less than) that found in local molecular clouds. This suggests that if the gas to dust ratio is normal, the CO abundance in this object is similar to that of clouds near the Sun.

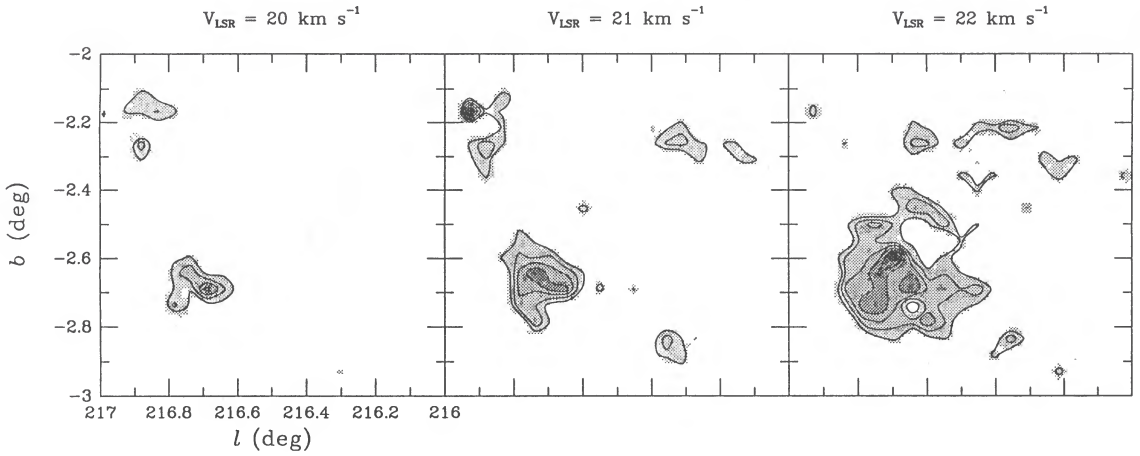

FIG. 3*a*

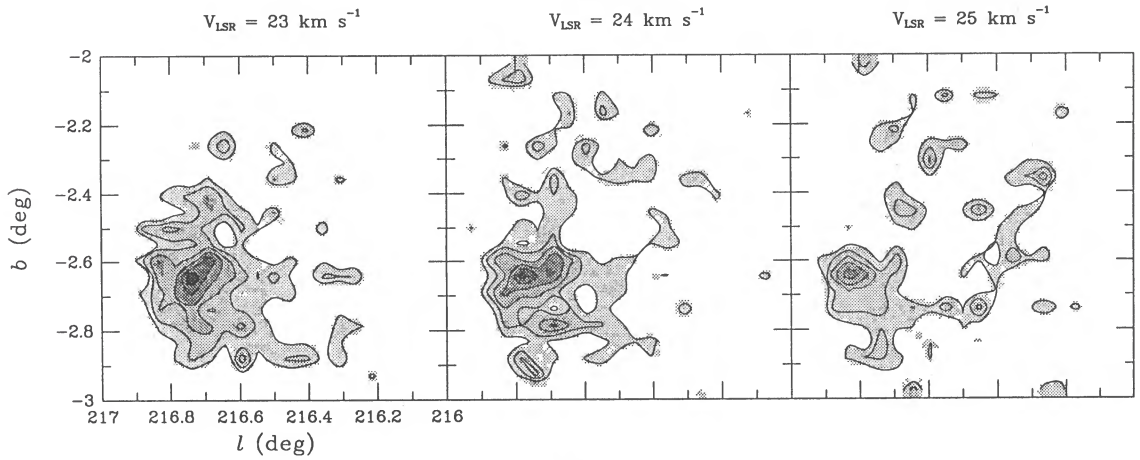

FIG. 3*b*

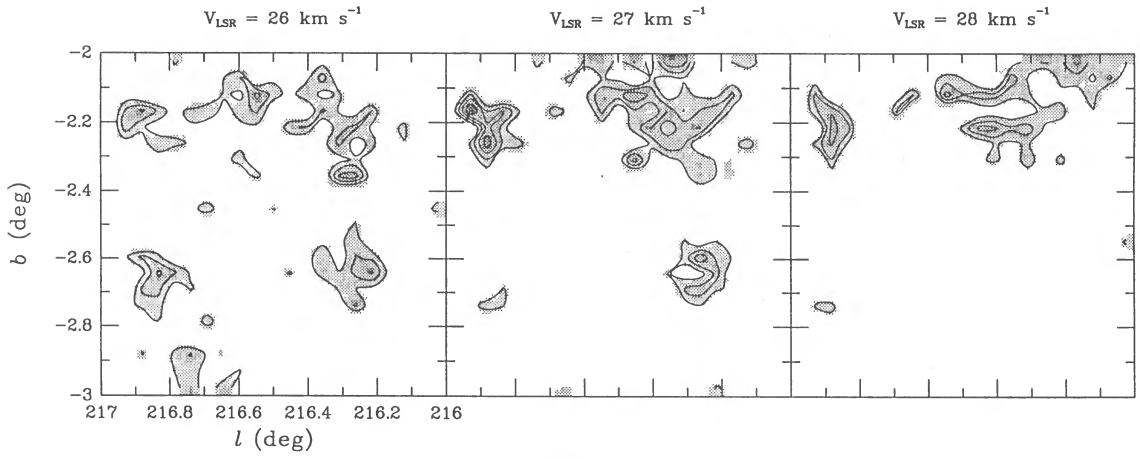

FIG. 3*c*

FIG. 3.—^{12}CO channel maps of the 1 deg^2 region of Maddalena's cloud with 3′ resolution; contour levels are 2, 2.5, ..., 4.5, 5 K. (*a*) V_{LSR} = 20 km s^{-1} (*left*), 21 km s^{-1} (*center*), and 22 km s^{-1} (*right*); (*b*) V_{LSR} = 23 km s^{-1} (*left*), 24 km s^{-1} (*center*), and 25 km s^{-1} (*right*); (*c*) V_{LSR} = 26 km s^{-1} (*left*), 27 km s^{-1} (*center*), and 28 km s^{-1} (*right*). Around 24–26 km s^{-1} ringlike structure is seen.

4.2. *Cloud Kinematics and Mass Discrepancy*

4.2.1. *Cloud Mass Estimates*

There is a big difference in the magnitudes of the masses derived by the virial technique and the LTE method. The virial mass is a factor of 8 larger than the LTE mass for the 0.25 deg^2 core region of the cloud. For the 1 deg^2 region which we mapped, the virial mass is a factor of 5 larger than the LTE mass.

A number of assumptions have entered into determining both the virial and LTE masses, including the ^{13}CO abundance and the density structure of the cloud. In an earlier study

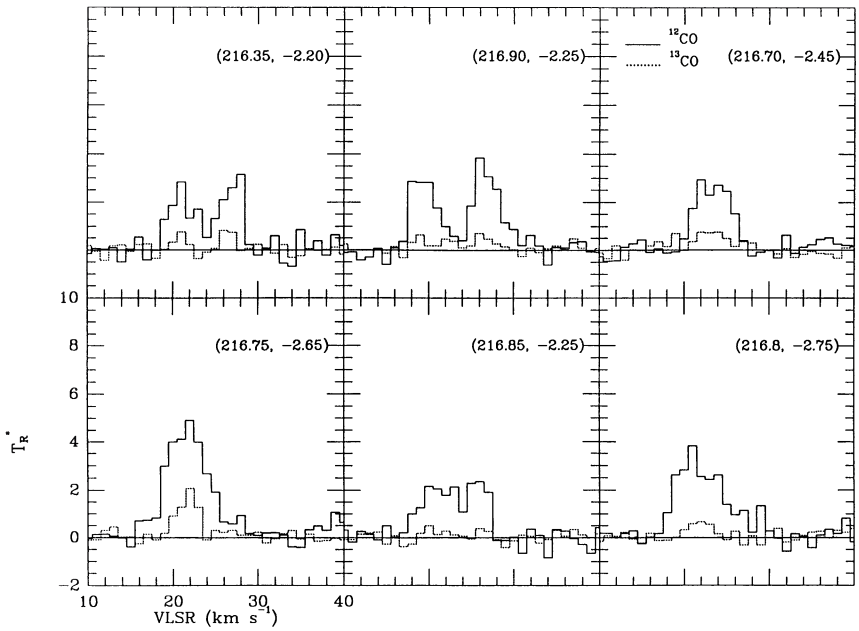

FIG. 4.—Some examples of typical spectra. Solid line represents ^{12}CO emission and dotted line represents ^{13}CO emission.

of GMCs in the inner Galaxy, Lee, Snell, & Dickman (1990) found a systematic difference between the LTE masses and the virial masses; however, this discrepancy was probably due largely to the difficulty in separating individual clouds in the crowded inner region of the Galaxy. In a study of outer Galaxy molecular clouds Carpenter, Snell, & Schloerb (1990) found good agreement between the virial and LTE mass estimates, suggesting than in well-resolved clouds these techniques give similar results. While the use of the virial expression may not be strictly applicable to small portions of a cloud complex, in the study of Carpenter, Snell, & Schloerb (1990) it was successfully applied to a single cloud that was part of much larger complex. Thus, one might expect relatively good agreement between the two mass estimates for Maddalena's cloud and the mass discrepancy is somewhat puzzling.

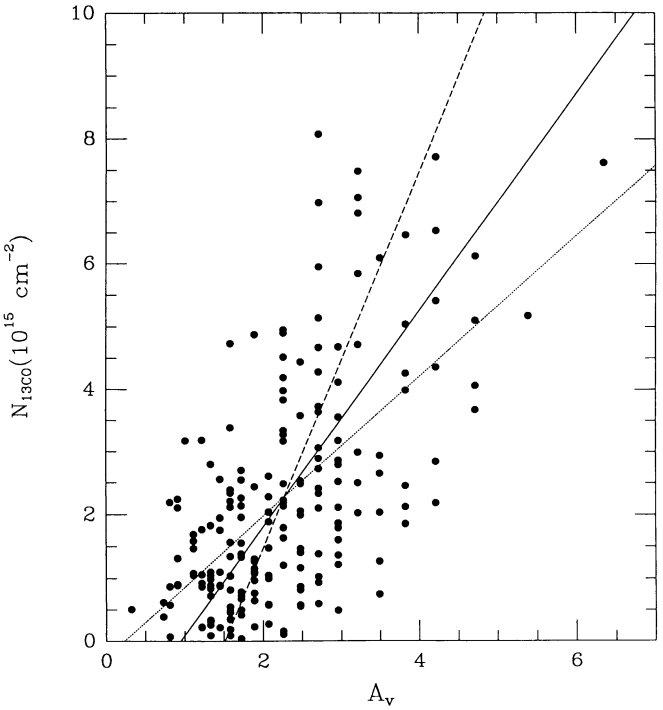

FIG. 5.—A_V–^{13}CO column density correlation. Dotted line represents a traditional least-squares fitted line (LSQ), dashed line is LSQ case when the axes of x and y are changed. Solid line represents the bisector of these two lines; its slope is 1.73×10^{15}.

A striking feature of Maddalena's cloud is the possible expansion of its central region at a velocity of approximately 4 km s^{-1}. Moreover, the dispersion of centroid velocities is nearly twice that of the average velocity dispersion along each line of sight. Thus, if the motions indicated by the shifts in the centroid velocity are not due to gravitationally bound motions, the virial mass will greatly overestimate the true mass that is present.

Therefore, if the central region of Maddalena's cloud is expanding and unbound, the mass discrepancy can be understood. However, the origin of these motions is not known. The total LTE mass of the expanding region is $2.5 \times 10^4\ M_\odot$ and its velocity is approximately 4 km s^{-1}. Thus, the total kinematic energy is 4×10^{48} ergs, which could be produced by a supernova explosion or winds from massive stars. However, there is no evidence for the presence of either massive stars or a supernova remnant in this region, although the expansion's dynamical time scale of approximately 3×10^6 yr is far greater than the visible lifetime of a supernova remnant. Further detailed mapping of the entire cloud is needed to determine if this explanation is correct.

4.2.2. CO *Luminosities versus Mass Ratio*

The ^{12}CO and ^{13}CO luminosities are calculated from $L = A\ \Sigma_i \Delta V_i \times T_{pk}^i$ [K km s^{-1} pc^2], where the sum is over all pixel i, ΔV_i is the full width at half-intensity in velocity units, and A is the pixel area in units of pc^2. The ^{12}CO luminosity is estimated as 0.57×10^4 K km s^{-1} pc^2 for the 0.25 deg^2 region, and 1.8×10^4 K km s^{-1} pc^2 for the 1 deg^2 region.

Empirical relationships between CO integrated intensity and H_2 column density, or between CO luminosity and mass,

TABLE 1

LEAST-SQUARES FITS OF $N(^{13}CO)$ VERSUS A_V FOR NEARBY CLOUDS

Cloud	Slope	Intercept	Distance (pc)	References
ρ Oph	2.5	...	160	Encrenaz et al. (1975)
L134	3.8	...	150	Tucker et al. (1976)
L43	1.5	...	160	Elmegreen & Elmegreen (1979)
Taurus	1.4	1.0	100	Frerking et al. (1982)
ρ Oph	2.7	1.6	160	Frerking et al. (1982)
	2.2	1.4	160	Dickman & Herbst (1990)
HCL2	1.3	0.5	100	Cernicharo & Guélin (1987)
L1495	2.0	0.5	100	Duvert et al. (1985)
Perseus	2.5	0.8	100	Bachiller & Cernicharo (1986)
Local clouds	1.9	...	...	Dickman & Clemens (1983)
This work	1.7	0.95	2200	

for GMCs in the inner Galaxy and for external galaxies have been found by a number of investigators and reviewed by Scoville & Sanders (1987). However, for the outer Galaxy this relation has been studied by only a few investigators (Sodroski 1990; Diegel, Bally, & Thaddeus 1990; Carpenter et al. 1990). The value for the inner Galaxy given by Scoville & Sanders (1987) is $N(H_2)/I_{CO} = 3.6 \times 10^{20}$ cm^{-2} (K km s^{-1})$^{-1}$ or equivalently, $M/L_{CO} = 7.9\ M_\odot$ (K km s^{-1})$^{-1}$ pc^{-2}. Lee, Snell, & Dickman (1990) found a ratio for the inner Galaxy of $N(H_2)/I_{CO} = 1.6$ to 2.8×10^{20} cm^{-2} (K km s^{-1})$^{-1}$ based on both LTE and virial mass determinations. For the outer Galaxy, Sodroski (1991) and Diegel et al. (1990) both found values considerably larger than those for the inner Galaxy; these range from 6 to 9×10^{20} cm^{-2} (K km s^{-1})$^{-1}$. However, Carpenter et al. (1990) also studied the ratio in outer Galaxy clouds that are luminous star-forming sites and found a ratio of 1.7×10^{20} cm^{-2} (K km s^{-1})$^{-1}$, much smaller than that found by the other investigators of the outer Galaxy and even slightly smaller than that found for the inner Galaxy. Thus, there is considerable uncertainty in the correct calibration of the CO intensity or luminosity to cloud column density or mass. In addition, it is not clear if there is a difference in the calibration factor between the inner and outer Galaxy. However, in the studies by Sodroski (1991) and Diegel et al. (1990), masses were derived by applying the virial theorem to rather poorly resolved molecular clouds, but even ignoring this issue, their masses are likely to be overestimated, since the spatial and velocity extents are in some cases implausibly large to correspond to single clouds.

For Maddalena's cloud, we can estimate the ratio between mass and CO luminosity. We use the LTE estimate for this purpose, since we have independently determined the ^{13}CO column density to A_V ratio. We find a LTE mass to CO luminosity ratio of 1.4 and 1.8 $M_\odot$ (K km s^{-1})$^{-1}$ pc^{-2} for the 1 deg^2 and the 0.25 deg^2 regions, respectively, or a ratio of $N(H_2)/I_{CO} = 0.7$ to 0.8×10^{20} cm^{-2} (K km s^{-1})$^{-1}$. The virial mass estimates lead to much larger ratios of $N(H_2)/I_{CO} = 3.1$ to 6.3×10^{20} cm^{-2} (K km s^{-1})$^{-1}$.

If the LTE masses are accurate, the conversion factor for Maddalena's cloud is unusually small. Theoretically, Dickman, Snell, & Schloerb (1986) found that for clouds in virial equilibrium the ratio between CO luminosity and mass depends on the temperature and density of the cloud in the following way:

$$M/L_{CO} \propto T^{-1}\rho^{-1/2}\ . \quad (5)$$

Since Maddalena's cloud is exceptionally cold, one might expect that it would have *less* CO emission per unit mass than warmer clouds, and thus a higher M/L_{CO} ratio than most clouds instead of the lower ratio our observations suggest. However, since the CO luminosity is given by $\sim T\Delta V\pi r^2$, if the cloud was larger than its equilibrium configuration, it would then have a *greater* luminosity for its mass. Likewise, since the virial mass is proportional to $r\Delta V^2$, if the cloud is expanding from an equilibrium configuration, one would also have an erroneously large virial mass. Thus, three pieces of evidence suggest that Maddalena's cloud may not be in virial equilibrium but instead in a state of expansion: (1) the large ratio of virial to LTE mass, (2) the small ratio of LTE mass to CO luminosity, and (3) the structure and kinematics of the cloud.

5. SUMMARY

We have observed emission from the $J = 1$–0 rotational transitions of ^{12}CO and ^{13}CO towards the inner portion of Maddalena's cloud in order to study the relationship between CO column density and visual extinction, and to derive various physical parameters of this unusual object. The visual extinction has been determined by traditional star counts. This represents the first detailed extinction map of a molecular cloud substantially beyond the solar neighborhood. The extinction distribution is in good agreement with that of ^{13}CO column density, and the slope of the correlation between these two parameters is estimated as 1.7×10^{15}. The ^{13}CO column density to visual extinction ratio is thus similar to that in local molecular clouds, suggesting that if the gas to dust ratio is normal, the CO abundance in this object is similar to that of the clouds near the Sun.

The masses derived from the LTE and virial analyses differ by a factor of 5 for the 1 deg^2 region; the virial analysis gives a mass 5 times larger than the LTE value. The structure and kinematics of the cloud inferred from the CO maps suggest that the inner region of the cloud resembles an expanding ring. Thus, both the kinematics of the cloud and the mass discrepancy suggest that this object may not be gravitationally bound. The large discrepancy in mass leads to a wide range of ratios of molecular hydrogen column density to CO integrated intensity, 0.7–6.3×10^{20} cm^{-2} (K km s^{-1})$^{-1}$. However, if we assume the LTE mass to be correct, the ratio would be 0.7×10^{20} cm^{-2} (K km s^{-1})$^{-1}$, much lower than that found for most GMCs in the inner Galaxy.

The Five College Radio Astronomy Observatory is operated with support from NSF grant AST 88-15406 and with permission of the Metropolitan District Commision.

REFERENCES

Bachiller, R., & Cernicharo, J. 1986, A&A, 166, 283
Bok, B. J., & Cordwell, C. S. 1973, in Molecules in the Galactic Environment, ed. M. A. Gordon & L. E. Snyder (New York: Wiley), 53
Carpenter, J. M., Snell, R. L., & Schloerb, F. P. 1990, ApJ, 362, 147
Cernicharo, J., & Guélin, M. 1987, A&A, 176, 299
Dickman, R. L. 1975, ApJ, 202, 57
———. 1978a, ApJS, 37, 407
———. 1978b, AJ, 83, 363
Dickman, R. L., & Clemens, D. P. 1983, ApJ, 271, 143
Dickman, R. L., & Herbst, W. L. 1990, ApJ, 357, 531
Dickman, R. L., & Kleiner, S. C. 1985, ApJ, 295, 479
Dickman, R. L., Snell, R. L., & Schloerb, F. P. 1986, ApJ, 306, 326
Diegel, S., Bally, J., & Thaddeus, P. 1990, ApJ, 357, L29
Duvert, G., Cernicharo, J., & Baudry, A. 1985, A&A, 164, 2
Elmegreen, D. M., & Elmegreen, B. G. 1979, AJ, 84, 615
Encrenaz, P. J., Falgarone, E., & Lucas, R. 1975, A&A, 44, 73
Feitzinger, J. V., & Spiker, J. 1987, A&A, 184, 122
Frerking, M. A., Langer, W. D., & Wilson, R. W. 1982, ApJ, 262, 590
Herbst, W., & Sawyer, D. L. 1981, ApJ, 243, 935
Isobe, T., Feigelson, E. D., Akritas, M. G., & Babu, G. J. 1990, ApJ, 364, 104
Kennedy, P. M., & Buscombe, W. 1977, MK Spectral Classifications (Evanston, IL: Northwestern University)
Kutner, M. C., & Ulich, B. L. 1981, ApJ, 250, 341
Lee, Y., Snell, R. L., & Dickman, R. L. 1990, R. L. 1990, ApJ, 355, 536
Maddalena, R. J., & Thaddeus, P. 1985, ApJ, 294, 231
Myers, P. C., Dame, T. M., Thaddeus, P. Cohen, R. S., Silverberg, R. F., Dwek, E., & Hauser, M. G. 1986, ApJ, 301, 398
Neckel, T., Staude, H. J., Meisenheimer, K., Chini, R., & Gusten, R. 1989, A&A, 210, 378
Penzias, A. A. 1975, in Atomic and Molecular Physics and the Interstellar Matter, Les Houghes 1974 (Session XXVI), ed. R. Balian, P. Encrenaz, & J. Lequeux (Amsterdam: North-Holland)
Scoville, N. Z., & Sanders, D. B. 1987, in Interstellar Processes, ed. D. J. Hollenbach & H. A. Thronson, Jr. (Dordrecht: Reidel), 21
Snell, R. L. 1981, ApJS, 45, 121
Sodroski, T. J. 1991, ApJ, 366, 95
Solomon, P. M., Sanders, D. B., & Rivolo, R. 1985, ApJ, 292, L19
Tucker, K. D., Dickman, R. L., Encrenaz, P. J., & Kutner, M. L. 1976, ApJ, 210, 679
van Rhijn, P. J. 1929, Groningen Publication 43
Wielen, R., Jahreiss, H., & Krüger, R. 1983, in IAU Colloquium 76, the Nearby Stars and the Stellar Luminosity Function, ed. A. G. D. Phillip & A. R. Upgren (Schenectady: Davis), 163